Nanoscale

Accepted Manuscript

This article can be cited before page numbers have been issued, to do this please use: S. Veeralingam and S. Badhulika, *Nanoscale*, 2020, DOI: 10.1039/D0NR03427D.

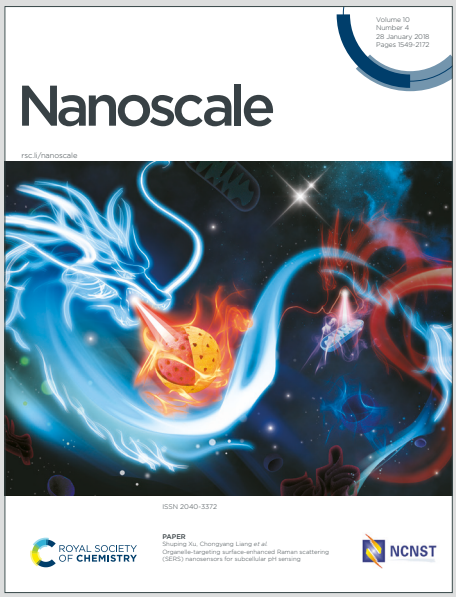

ROYAL SOCIETY OF CHEMISTRY

rsc.li/nanoscale

DOI: 10.1039/D0NR03427D

X (Metal: Al, Cu, Sn, Ti) - functionalized tunable 2D-MoS_2 nanostructures assembled biosensor array for qualitative and quantitative analysis of vital neurological drugs

Sushmitha Veeralingam[1], and Sushmee Badhulika[1]*

[1]Department of Electrical Engineering, Indian Institute of Technology Hyderabad

Hyderabad, 502285, India

**Corresponding author: E-mail: sbadh@iith.ac.in; Telephone: 040-23018443 Fax 04023016032*

Abstract:

In this work we report for the first time surface functionalization of 2D MoS_2 with X (Metal : Al, Cu, Sn, Ti) to develop a low-cost, ultra-selective biosensor array based Electronic Tongue (E-Tongue) for detection of 4 vital neurological drugs in human saliva. The hydrothermally grown surface functionalized X-MoS_2 were integrated onto a single 1 x 1 cm aluminium foil and contacts were defined using Cr electrodes. Detailed characterization revealed the formation of 2-H MoS_2 and metal-X (Al, Cu, Sn, Ti) - functionalized MoS_2 nanoflowers like morphology decorated with nanoflakes, nanorods, nanocubes and nanosticks structures respectively. The response of the sensor array was recorded for Aspirin, Nicotine, Caffeine and Tramadol. Principal Component Analysis (PCA) was employed to reduce the dimension of numerous response data set from all sensors and predicts the likely possible response from various neurological drugs towards each sensor. The pattern-recognition analysis confirmed a definite pattern in response for respective functionalization and could efficiently differentiate neurological drugs from one another. Real-time analysis was done using saliva samples for monitoring the therapeutic neurological drug concentration in human body. Further the biosensor array was exposed with respective neurological drugs to study the sensitivity,

View Article Online
DOI: 10.1039/D0NR03427D

selectivity, stability, reproducibility and adhesion on the of the device. The strategy outlined can be used to develop lab-on-a-chip devices for real-time detection of numerous bio analytes in body fluids.

Keywords: biosensor array, MoS_2, metal functionalization, neurological drugs, Saliva samples

Introduction:

Quantitative analysis of neurological drugs is crucial as the kinetics of the body fluids is highly dependent on the concentration of drugs. The analysis of neurological drugs is important due to the major disorders associated with it like epilepsy, Parkinson's disease, Alzheimer's disease, hepatic and renal disorders [1]. Studies also state that few neurological drugs play's a major role in affecting the rate of metabolism of vital organs of the body like livers and kidneys leading to many acute and chronic diseases.[2]. Therefore, it is essential to fabricate a low cost, scalable, highly selective, biosensor array-based devices for simultaneous detection the neurological drugs.

Analysis of neurological drugs has been carried out previously using spectrophotometry, gas or liquid chromatography, fluorometry, potentiometric techniques [3]. Limitation posed by these techniques were excessive sample preparation steps, inefficient data arising from interfering species, and lack of simultaneous drug detection. In this regard, simultaneous sensing is a necessary pre-requisite for real-time detection of complex analytes in body fluids like saliva, sweat etc [4]. Biosensors for simultaneous detection of multiple analytes are categorised into (i) the multi-label and (ii) the multi-electrode platforms. The issues with multiple-electrode platforms include i) multiple and extensive sample synthesis and analysis ii) different sensing setup iii) cross-reactivity and expensive branched conductive channels through all electrodes. Further, multi-label systems are also important in the selective detection

of multiple bio-analytes. Among this, enzyme-based and metal-based labels have frequently been used for the amplification of the signals obtained from the different analytes. However, the obtained signals by the enzymatic reactions are not adequate and often fail to reach the low detection limit. However, the metal-ions based label have proven to produce excellent sensitivity and ultra-low-limit of detections owing to the enhanced adsorption and quicker electron transfer. Hence, metal- labeled selective, flexible biosensors are the most suitable for facile, real-time, and simultaneous detection of neurological drugs based wearable biosensors.

2D TMDC's (Transition metal dichalcogenides) materials have been widely used for electrocatalytic detection-based applications. The reduced dimension and higher integration density of TMDCs facilitates modification strategies like functionalization and doping [6] which helps in tuning the electronic properties of the material, making TMDCs very attractive for sensing. Surface functionalization using lewis acid :base reaction enables the precise control of electronic states of 2D-materials by interacting with the dangling bonds present in 2D materials.[7]. Functionalization allows the coexistence of nanostructures and nanomaterials [8] on the surface which improves the versatility of the 2D material. This stable strategy tunes the fermi level of the 2D material by modifying the surface states due to molecular functionalization with metals. The surface modification improves the scalability and integration of nanomaterials to a single device. Moreover, this method of surface functionalization provides chemical stability and defect free chemical synthesis of functionalized 2-D materials which can widen the applicability in simultaneous detection of various analytes [9].

In this work, we report a low cost, flexible X-functionalized MoS_2 based highly selective biosensor array for detection of neurological drugs in human saliva. Initially, MoS_2 and X (Al,

Cu, Sn, Ti)- functionalized MoS_2 was directly grown on flexible aluminium foil using a facile one-step hydrothermal method. Unlike polymer-based substrates, Aluminium is impermeable to H_2O or O_2, can withstand high processing temperatures, recyclable and has excellent dimensional stability [10] making it highly suitable for sensing applications. The hydrothermally grown surface functionalized X-MoS_2 were integrated onto a single aluminium foil and proper contacts were defined using thermal evaporation technique. Detailed characterization of the biosensors was carried out using XRD (X-ray diffraction technique), FESEM (Field emission scanning electron microscopy), EDAX (Energy dispersive X-ray analysis) and Raman spectroscopy. The sensor array was exposed to 0.1 μM concentration of neurological drugs, the results were analysed using normalised resistance plots and PCA analysis. From PCA analysis it was observed that Al – functionalized MoS_2 (Al- MoS_2) showed very high response towards aspirin. Similarly, Cu functionalized MoS_2 (Cu-MoS_2), Sn-Functionalized MoS_2 (Sn-MoS_2), Ti – functionalized MoS_2 (Ti-MoS_2) were selective towards caffeine, tramadol and nicotine respectively. The real-time detection of the analytes was carried out using saliva because major amount of organic and inorganic substances, neurological drugs and their metabolites are secreted in saliva. Moreover, collection of saliva is easy and diagnosis is safe for patients and health professionals. The sensitivity, selectivity, stability and reproducibility for X-MoS_2 have been verified with various concentration of neurological drugs to obtain their respective dynamic range (DR), limit of detection (LOD) and sensitivity. Further, the nanoparticles had excellent adhesion towards aluminium substrate which is evident from the scotch cape test as shown in attached SI S2. video file. To the best of authors' knowledge, this is the first demonstration of low cost, flexible sensor array for detection of neurological drugs in human saliva.

Experimental details:

Fabrication of X- MoS_2 array device: -

View Article Online
DOI: 10.1039/D0NR03427D

The neurological drug biosensor array was fabricated by integrating four different metals i.e. X- (- Al, Cu, Sn, Ti) functionalized MoS_2 onto a single 1 cm x 1 cm flexible aluminium foil. The hydrothermally grown X- decorated MoS_2 as shown in figure 1(a) was carefully placed over the aluminium foil such that the planar contacts can be taken from the sides of the biosensor array. Further, to achieve the planar contacts, masking was done on the sensor surface using predesigned polyimide mask. Aluminium contacts were thermally evaporated on the edges of the sensor array as depicted in the figure 1(b). The thermal evaporation was carried in a high vacuum chamber at a pressure of 5.0 x 10^{-6} m bar for 60 sec with a deposition rate of 24.0 nm s^{-1}. The biosensor array was carefully removed from the evaporation chamber and the predefined masks were carefully removed for further usage in detection of neurological drugs.

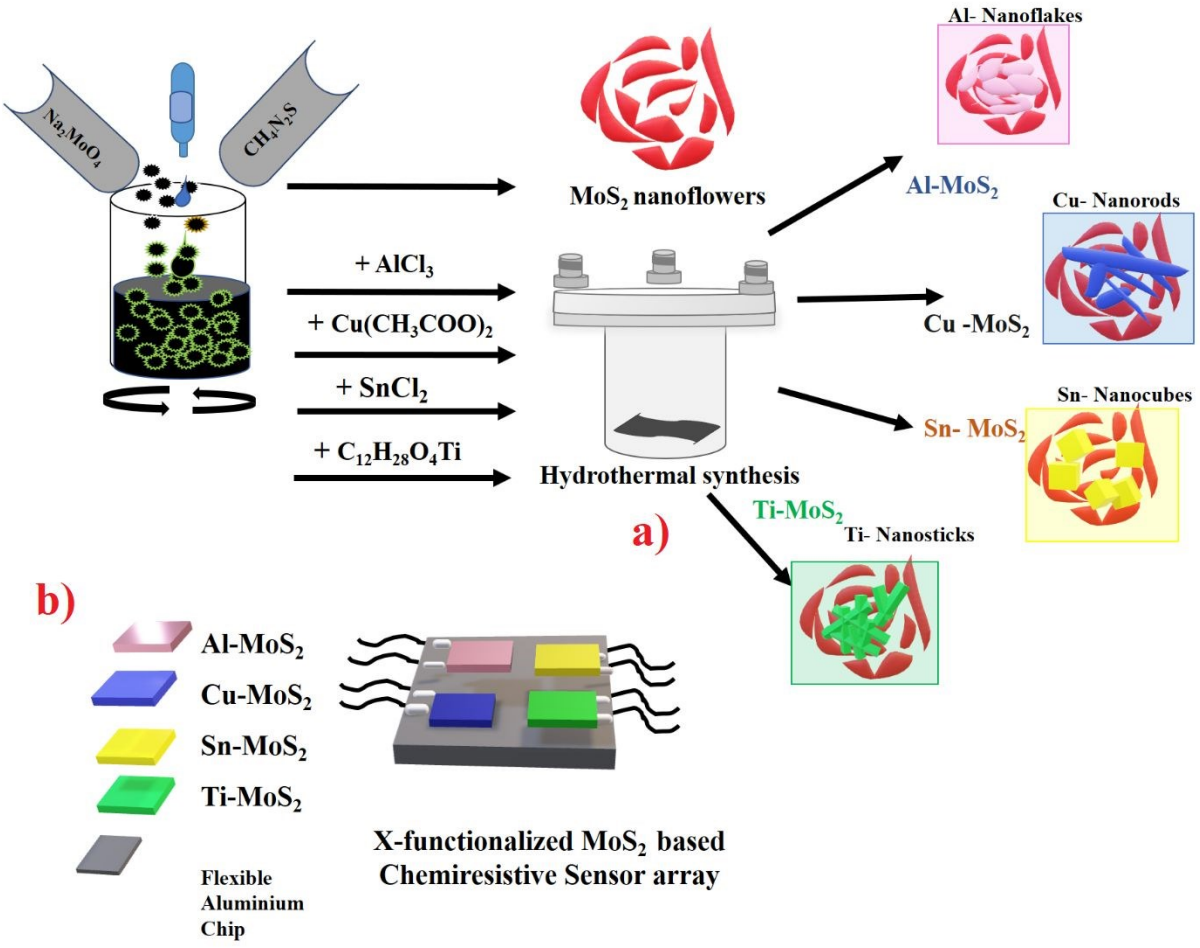

View Article Online
DOI: 10.1039/D0NR03427D

Figure 1(a). Synthesis of X- functionalized MoS_2 (Al, Cu, Sn, Ti) using facile, one step hydrothermal method. (b) Fabrication of X- functionalized MoS_2 biosensor array.

Results and discussion:

Morphological and Structural studies

The morphological studies of hydrothermally grown pristine MoS_2 and X- functionalized MoS_2 were carried out using FESEM studies. Figure 2(a) displays the lower magnification images of pristine MoS_2 depicting the uniform growth of MoS_2 nanoflowers on the aluminium substrate. The higher magnification images of MoS_2 nanoflowers can be seen in figure 2(b). The diameter of the MoS_2 flowers were in the range of 200 nm – 280 nm. The petal like structures were measured to be in the range of 5 - 60 nm, thus providing high surface area and electrocatalytic sites for the detection of neurological drugs. Figure 2(c) displays the higher magnification image of Al-MoS_2. The aluminium atoms were found to form nanoflake like structure over the surface of MoS_2. The nanoflakes were found to be randomly distributed on the surface of MoS_2 nanoflowers which indicates the simultaneous presence of both Al nanoflakes and MoS_2 nanoflowers attributing to the encapsulation of MoS_2 nanoflowers on the aluminium substrate and further preventing agglomeration and forming nanoflakes like structure. [11] of aluminium chloride among the other relevant precursors used during hydrothermal growth. The higher magnification images of Cu-MoS_2 depicts the formation of nanorods like structure on the surface of the MoS_2 nanoflowers. The Cu atoms were found to form nanorod like structures as shown in figure 2(d). The diameter of the nanorods where found to be approximately in the range of 20 - 80 nm. The formation of nanorods can be attributed to the surface confined growth method [12]. A MoS_2 layer was seed coated over aluminium substrate and Cu nanorods where observed to be grown randomly filling the gaps of the confined nanoflower like structure. Figure 2(e) displays the functionalization of Sn nanocubes on the surface of MoS_2 nanoflowers.

View Article Online
DOI: 10.1039/D0NR03427D

Sn atoms were observed to be in perfect cubic shape bounded with sharp corners and edges embedded on the surface of MoS_2 nanoflowers. The average size of the nanocubes were found to be ~ 190 nm. The formation of Sn nanocubes can be attributed to the surfactant free hydrothermal conditions. Previous reports [13] suggest that surfactant assisted growth leads to the formation of agglomerated Sn atoms, which further reduces the surface area of the nanoparticles, hence in this report a surfactant free Sn functionalization was carried out. Figure 2(f) displays the formation of vertically grown Ti nanosticks on the surface of the MoS_2 nanoflowers. Highly oriented nanosticks were grown on the nanflower like structure. The length of the nanosticks were in the range of 600 – 700 nm and the width were found to be in the range of 50- 80 nm. The growth of the nanosticks was found to be in the c- axis which can be attributed to the uniform hexagonal atomic configuration of Ti and MoS_2 providing possibility of growing vertical nanosticks [14] over nanoflowers. It is evident from the low magnification FESEM images (shown in SI figure S1) that the X-MoS_2 was grown uniformly over the surface of the aluminium foil. It should be noted that the aluminium substrate acts as a flexible substrate for uniform growth of the nanostructures and doesn't influence the sensing mechanism. The adhesion property was further verified using the facile scotch tape test as shown in SI. S2 video file.

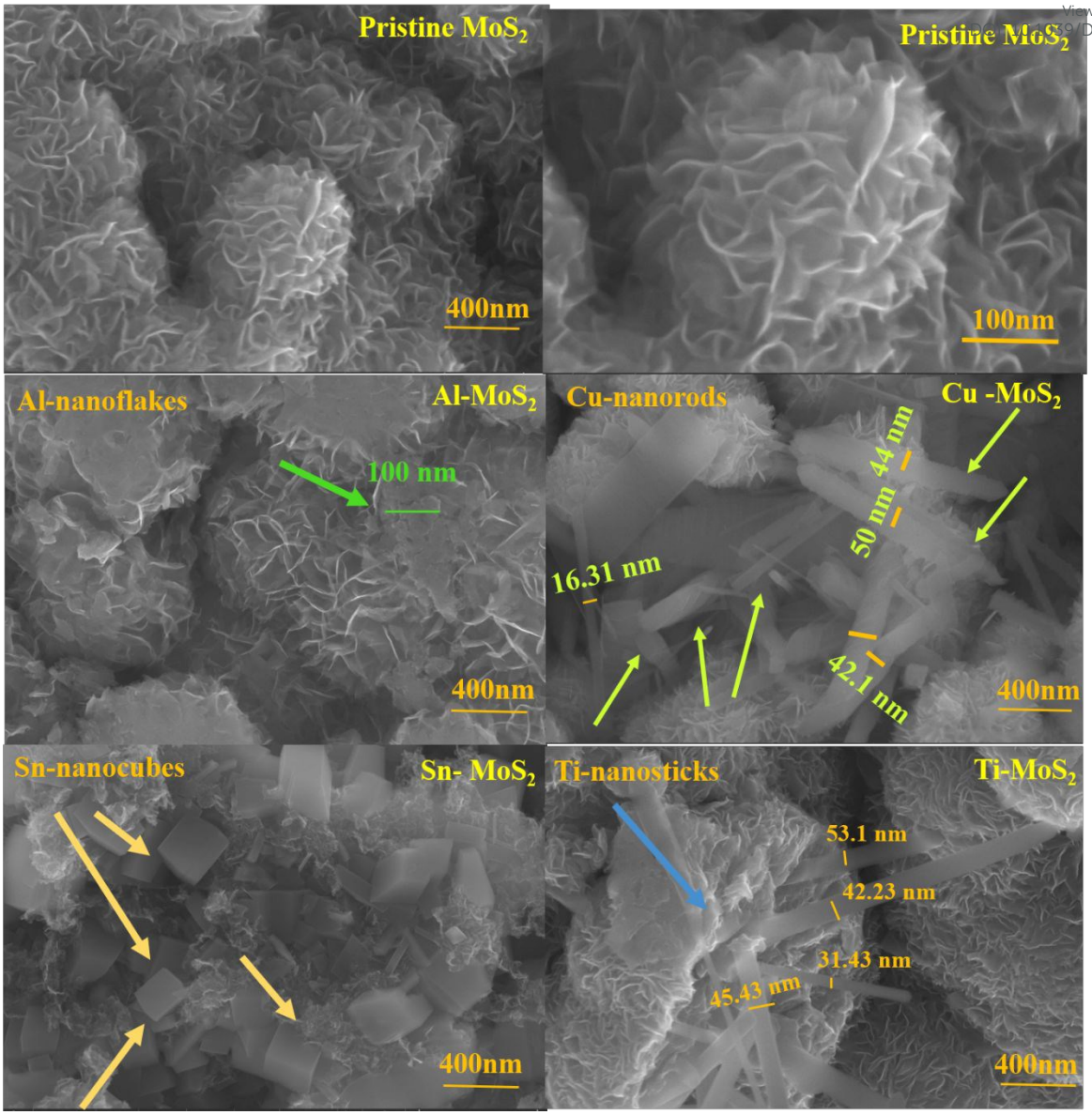

Figure 2. FESEM studies depicting (a) lower magnification of pristine MoS_2 (b) higher magnification images of pristine MoS_2 ; Higher magnification images of (c) Al- MoS_2 (d) Cu- MoS_2 (e) Sn-MoS_2 (f)Ti-MoS_2.

XPS analysis have been performed for pristine MoS_2 nanostructures and given in Figure S2(a). The peaks around 228 eV and 231 eV can be assigned to the 3d5/2 and 3d3/2 states of in Mo. The deconvoluted peaks at 229 eV and 233 eV can be attributed to 2H phase of semiconducting MoS_2. Figure S2(b) illustrates the XPS spectra of S2p, the obtained peaks at 162 eV and 163 eV represents the S2p 3/2 and S2 p1/2 states of the sulphide. The formation of hexagonal MoS_2 can be validated from the obtained XPS studies [15].

View Article Online
DOI: 10.1039/D0NR03427D

Further, EDAX analysis was carried to identify the elemental composition of MoS_2 and X-functionalized MoS_2 as shown in Table 1. The EDAX studies of pristine MoS_2 revealed the presence of molybdenum and sulphur atoms in 1:0.62 ratio. The stoichiometric ratios were consistent with the previous reports [16]. The possible reaction for the formation of MoS_2 is given in eqn. 1:

$$\mathbf{Na_2MoO_4.2H_2O + 2\ CH_4N_2S = MoS_2 + 4\ NH_3\uparrow + 2\ NaCO_3} \qquad \mathbf{-1}$$

Where, MoS_2 was found to be the resultant product of the hydrothermal synthesis and the by-product NH_3 gets evaporated while $NaCO_3$ gets completely dissolved in the DI water solvent. It was also found that aluminium foil does not take part in any chemical reaction and aids in uniform growth MoS_2 all over the surface. Further, the details on optimization of doping % is given in SI section S3 and Figure S3. The at. % of aluminium was found to be 8.63 % in Al-MoS_2 whereas at. % of Cu was found to be 9.21%. The at% of Sn and Ti were found to be 7.25 and 6.39 respectively. The obtained atomic percentages correspond to the functionalization of 2D-MoS_2. The EDAX maps are shown in figure S4. The functionalization of Al^{3+}, Cu^{2+}, Sn^{4+}, Ti^{4+} on 2D-MoS_2 can be attributed to the Lewis acid-base reaction which does not modify the host 2D structure. The sulphur atoms of MoS_2 on the surface end with a lone pair of electrons forming a Lewis base which is ready to react with any lewis acid complexes like Al^{3+}, Cu^{2+}, Sn^{4+}, Ti^{4+}. This is the valid approach for surface functionalization of 2D-materials.

Table 1. EDAX studies of Pristine MoS_2 and X- functionalized MoS_2

X - doped MoS_2	Mo	S	X doping

	Weight %	Atomic %	Weight %	Atomic %	Weight %	Atomic %
MoS_2	67.38	40.68	32.40	59.24	-	-
Al – MoS_2	62.38	36.40	28.40	54.50	9.22	8.63
Cu- MoS_2	61.84	38.68	30.05	52.58	8.11	9.21
Sn- MoS_2	59.38	39.43	34.40	51.59	6.22	7.25
Ti – MoS_2	64.38	34.12	30.40	57.6	5.22	6.39

The structural characterisation of hydrothermally grown pristine-MoS_2 and X-MoS_2 were carried out using XRD studies as shown in figure 3(a). The diffraction peaks of MoS_2 were seen at 14°, 44°,65°,78° corresponding to (002), (004), (006), (008), (0010) planes thus, can be indexed to hexagonal phase of MoS_2 with a JCPDS no. 37-1492 [17]. Further, these peaks were prominent in all the X- MoS_2 along with the functionalized metal (Al, Cu, Sn, Ti) peaks. The diffraction peaks of Al-MoS_2 were seen at 38°, 45°, 65° corresponding to the (111), (200), (220) planes. The peaks can be indexed to cubic phase of Al [18]. Cu-MoS_2 was found to have diffraction peaks at 40°, 51° corresponding to (111), (200) planes in addition to MoS_2 diffraction peaks which can be indexed to cubic phase of Cu [19]. The disappearance of diffraction peak at 14° for Cu-MoS_2 can be attributed a) to the change in number of layers of MoS_2 b) amorphization of the sample due to surface functionalization of Cu^{2+} and c) disordering of the original crystalline structure of MoS_2 [20]. For Sn- MoS_2, the diffraction peaks were found at 32°,35°,38°,57° corresponding to (110), (100), (200), (211) planes. The obtained peaks can be indexed to tetragonal phase of Sn [21]. The diffraction peaks of Ti-MoS_2 were found at 33°,38°,49°,58°,60°,69° corresponding to (0001), (2-1,-1,0), (2,-1,-1,1), (2,0,-2,1), (0,0,0,2),(3,0,-3,0) planes which can be indexed to the hexagonal phase of Ti [22]. The Raman spectrum of MoS_2 nanoflowers as illustrated in figure 3(b) were found to be in agreement with the XRD results depicting the formation of 2H- MoS_2. The two prominent Raman bands were observed at ~381.3 cm^{-1} and ~405.8 cm^{-1}, which can be ascribed to E^1_{2g} and

View Article Online
DOI: 10.1039/D0NR03427D

A_{1g} vibrational modes [23]. The E^1_{2g} band corresponds to the in-plane vibration of S atoms and A_{1g} mode corresponds to the out-of-plane vibration of S atoms relative to Mo atom. The Raman frequency difference between E^1_{2g} and A_{1g} modes were found to be 24 cm^{-1} which corresponds to the frequency of few layers of MoS_2. The in-plane and out-of plane vibrations helps to understand the restricted two modes of vibration, which is achieved at the best in 2D materials. It was found that the functionalization of MoS_2 didn't change the number of layers of MoS_2. Moreover, no significant Raman bands were found for Al- MoS_2 and Cu-MoS_2 due to the absence of optical phonon modes. Al, Cu, Sn and Ti are metallic in nature having only acoustic modes of vibration. Raman analysis involving electron–phonon interactions can also be used to interpret the electron state changes. The E^1_{2g} band and A_{1g} band are consistent in functionalized MoS_2 structure suggesting stable lattice structure. However, the attenuation of peak intensity for X-functionalized MoS_2 can be attributed to the mismatched resonant condition possibly due to electron-pulling effect, as fewer electrons are available for raman process.

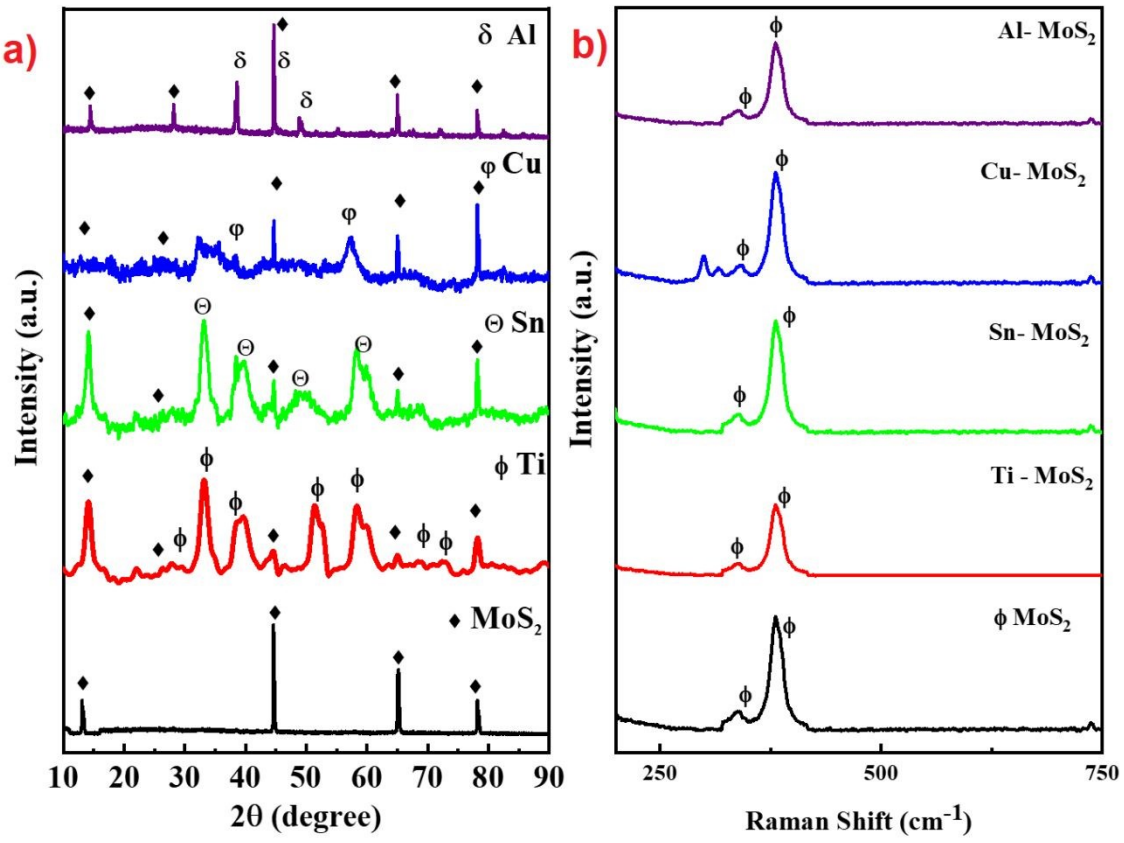

Figure 3. a) XRD studies of pristine - MoS_2 and X (Al, Cu, Sn, Ti)-MoS_2 b) Raman studies of pristine - MoS_2 and X (Al, Cu, Sn, Ti)-MoS_2.

X- MoS_2 based biosensor array:

The I-V characteristics of pristine MoS_2 and surface functionalized X(Al, Cu, Sn, Ti)-MoS_2 was separately carried out as shown in SI figure S5. to understand the electronic properties of X-MoS_2. Increase in current was found for Ti-MoS_2 when compared to pristine MoS_2. This can be attributed to the increase in carrier concentration and fermi level shift with Ti doping. Further, the current was found to decrease for Al-, Cu, Sn -MoS_2. The decrease in current corresponds to the shifting below of fermi-levels due to the withdrawal of electrons from MoS_2. The observed results was also consistent with the carrier concentration obtained from hall-effect measurements as given in SI section S3. The fabricated biosensor array-based e-tongue was used for detection of the neurological drugs namely, aspirin, caffeine, tramadol and nicotine dispersed in buffer solution of pH - 7.2. It should be noted that the pH of the buffer solution was optimized as detailed in SI Section S4 and figure S6. The concentration of AS, CF, TR and NC were maintained as 0.1 µM. The prepared solution was spiked on to the MoS_2 and biosensor array and corresponding resistance was calibrated using normalised resistance values. The resistance of each biosensor was obtained in the air (R1) and was also obtained after the spiking (R2) of all the drugs. The normalized resistance was calculated by using the formula - (R2-R1/R1). The results obtained are shown in figure 4(a). It was observed that MoS_2 is least selective towards the neurological drugs, this can be attributed to the absence of binding sites of the ion or molecule to form coordination complex. From the studies, it was also observed that Al-MoS_2 was highly selective towards aspirin, Cu -MoS_2 towards caffeine, Sn-MoS_2 towards tramadol, Ti-MoS_2 towards Nicotine. The selectivity can be attributed to the binding of the ion or molecule that forms a coordination complex with the metal atoms and displays excellent electron transport with the specified metal surface. Thus, Al-MoS_2 displays

an enhanced normalised resistance with the aspirin and similarly for the other metal ions towards the drug molecules. The metal functionalization gives better specificity towards the neurological drugs. Each neurological drug displayed a distinct response and pattern for identification, combined with chemometric analysis. The mechanistic study for sensing was done using chemiresistive measurements and revealed that the sensing mechanism of the Al functionalized MoS_2 towards neurological drugs was governed by the charge transfer mechanism, whereas the Sn, Ti and Cu functionalized MoS_2 hybrid device was governed by electrostatic interaction and oxidation effects in combination. Further, the recorded electronic responses for all hybrid sensors were analysed using a pattern-recognition analysis tool like PCA. The selectivity pattern was also further studied with the help of a multivariate statistical technique called principal component analysis.

Principal Component analysis:

To identify the performance of X-MoS_2 e-tongue array towards neurological drugs a simple statistical analysis called Principal component analysis (PCA) was employed. The set of observations for possibly correlated variables among different dimensions i.e the response of the X-MoS_2 biosensor array towards various neurological drugs can be obtained using PCA. A matrix of data was devised where the columns were recorded as the normalised resistance values obtained from X-MoS_2 biosensors (Al-MoS_2, Cu -MoS_2, Sn- MoS_2, Ti-MoS_2) and the rows represented the measurement of neurological drugs. In this case the first two principal components accounted for 44.8 % and 36.08 % of the variance. The observations were analysed by plotting the graph between the principal component 1 (PC 1) and principal component 2 (PC 2). The data points obtained from the AS, CF, TR and NC were aggregated in different regions, which can be assigned to the specific sensing pattern of the neurological drugs. The obtained variance of PC 1 vs PC 2 plots values representing each neurological drug were grouped together. The distribution of data points was distinct with no overlapping. The

separation between the distributed data points corresponding to each neurological drug is shown in figure 4(b). The overall PCA profile represents a high selective detection of the neurological drugs towards metal functionalized 2D MoS_2.

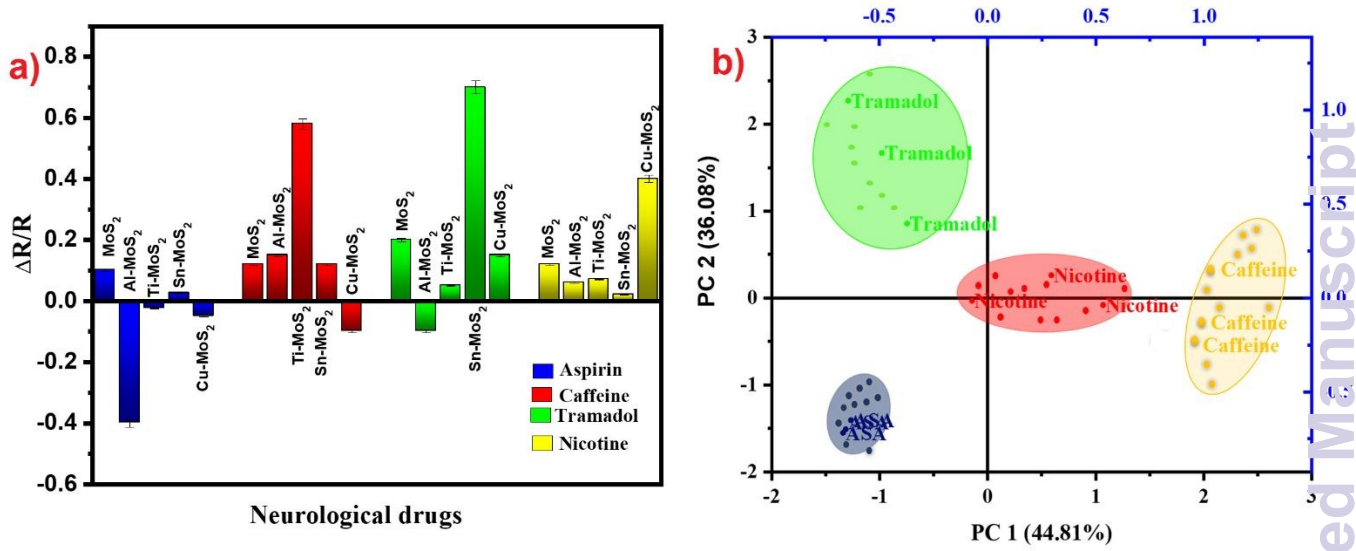

Figure 4. a) The normalised resistance of X- functionalized MoS_2 towards the 4 neurological drugs for n = 5 devices. b) PCA analysis obtained for sensor array towards AS, CF, TR and NC.

AS, CF, TR and NC sensing: -

Functionalized 2D- nanomaterial based detection systems provide novel electrical properties based sensing startegy. Quantitative sensing studies of neurological drugs like AS, CF, TR and NC were carried out with functionalized 2D-MoS_2 biosensor array. It was evident from PCA analysis that Al-MoS_2, Cu-MoS_2, Sn-MoS_2 and Ti-MoS_2 were highly selective towards AS, CF, TR and NC respectively. Hence, the sensing studies where carried out with the help of C-V (current vs voltage) characteristics on Al-MoS_2, Cu-MoS_2, Sn-MoS_2 and Ti-MoS_2 sensor respectively. Also, the I-V characteristics for various concentration of AS, CF, TR and NC towards MoS_2 were performed on a pristine MoS_2 device with Cr as contacts as shown in figure

S7. The physiological relevant range of AS secreted in saliva was reported as 0.2 - 2 μM [24]. Hence, the relevant concentration of AS (0.01 μM – 50 μM) within physiological range was prepared in PBS of pH- 7.2. The response of Al-MoS_2 based biosensor was obtained by periodically spiking the prepared different concentrations of AS on the sensor. The current vs voltage studies were initially taken for Al-MoS_2 biosensor in the RT ambiance conditions followed by spiking of various concentration of AS. A standard standby time of 5 minutes was given before recording the I-V experiments to obtain a stabilized response. Figure 5(a) displays the I-V response of the fabricated Al-MoS_2 nanoflakes based e-tongue towards increase in concentrations of AS. The current flowing through the biosensor was found to decrease with the increase in concentration of AS. This can be attributed to the reduction of AS to salicylic acid by accepting electrons from the surface [25] of Al-MoS_2 as shown in figure 5(b). AS, also known as acetylsalicylic acid evidently contains excess of H^+ ions which tends to withdraw the electrons from the surface of n-type Al-MoS_2 upon interaction. When higher concentrations of AS. were spiked on the surface of Al-MoS_2 nanoflower – nanoflake like structures, AS tends to interact with the active sites in the biosensor withdrawing electrons from the sensor which decreases the current flowing through it.

Increase in levels of CF in the range of 0.4 μM- 1 μM in saliva was a minor indication of either Dementia/Alzheimer's disease or cardiovascular diseases [26]. Hence, CF was taken in the range of 0.01 μM – 10 μM for sensing towards Cu-MoS_2. Figure 5(c) depicts the I-V characteristic response of bare Cu-MoS_2 biosensor in air followed by successive spiking of increase in concentration of CF from 0.01 μM – 10 μM on the Cu-MoS_2 biosensor. The results displayed an increase in trend of current with increase in concentration of CF. This can be attributed to the oxidation of CF to 1,3,7 – trimethyluric acid [27], where CF donates electrons to the Cu-MoS_2 biosensor and oxidises to 1,3,7 – trimethyluric acid as shown in figure 5(d). With the increase in concentration of CF, more CF atoms gets oxidised in presence of Cu

nanorods on the surface of MoS_2 nanoflower with enhanced interaction sites of the biosensor the current was found to further increase. The current enhancement was observed as 3.8 mA with the spiking of CF when compared to the bare Cu-MoS_2 as a clear evidence for catalytic oxidation of Cu-MoS_2 towards CF.

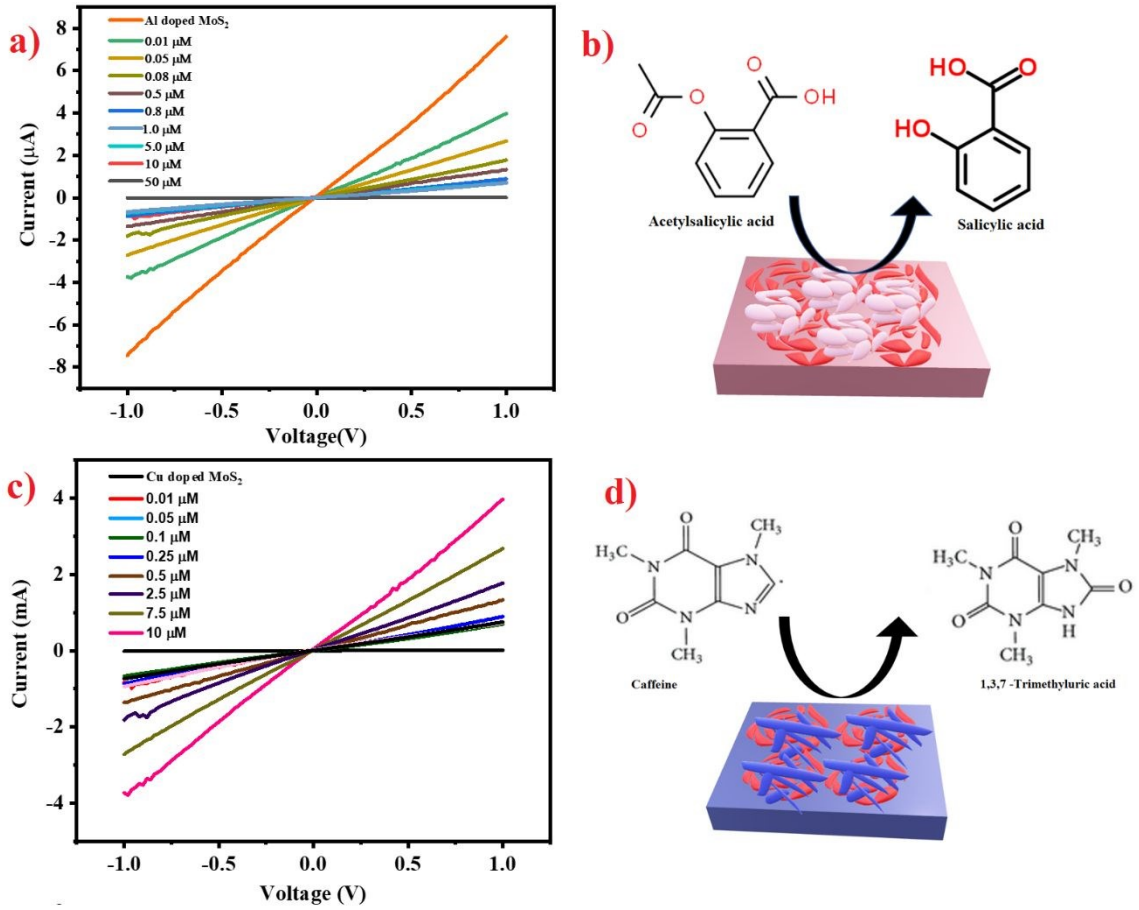

Figure 5 (a) I-V characteristics for various concentration of AS towards Al-MoS_2 b) sensing mechanism describing the reduction of acetylsalicylic acid to salicylic acid(c) I-V characteristics for various concentration of CF towards Cu-MoS_2 (d) sensing mechanism describing the oxidation of caffeine to 1,3,7 -trimethyluricacid

Supra-therapeutic doses of TR precipitated in saliva for the range 1-1.5 µM accounts for major disorders like cardiovascular collapse, seizures, and respiratory depression up to respiratory arrest [28]. Hence, detection of TR in the range of 0.01 µM -1.5 µM was performed for Sn-

View Article Online
DOI: 10.1039/D0NR03427D

MoS_2 biosensor. Figure 6(a) depicts the I-V studies for Sn-MoS_2 and response of Sn-MoS_2 towards increase in concentrations of TR. The I-V responses were recorded for bare Sn-MoS_2 following the successive increase in concentration of TR. Initially, bare Sn-MoS_2 biosensor displays a current of 0.9 nA but with increase in TR concentration an enhancement of current up to 2.6 nA was observed. The increase in current flowing through the sensor can be attributed to the oxidation of TR to O, N – didesmethyltramadol [29].TR tends to oxidise and lose electrons in presence of electroactive and TR selective Sn nanocubes to form O, N – didesmethyltramadol as shown in figure 6(b). With increase in concentration of TR from 0.01 μM -1.5 μM, excess electrons are donated to Sn-MoS_2 attributed to the increase in oxidised TR molecules. Increase in current with spiking of Sn-MoS_2 exhibits a clear evidence of oxidation of TR in presence of Sn-MoS_2.

Nicotine is widely used as therapeutics for smoking disorders. The physiological harmful range of nicotine precipitated in saliva is 0.5 μM – 0.8 μM [30]. Hence, it is crucial to detect ultra-low concentration of nicotine in saliva. The I-V studies were obtained by successive spiking of prepared concentrations of NC from 0.01 μM – 10 μM on the biosensor. Figure 6 (c) displays a stable increase in current with the increase in NC concentration, which can be attributed to the oxidation of NC in presence of Ti-MoS_2 to narcotinine [31] as displayed in figure 6 (d). NC donates electrons to the Ti-MoS_2 while interacting with titanium nanostick like structure, which provides an enhanced surface area and selective active species for sensing of the NC. The increase in current can also be attributed to the increase in active sites forming unique morphology for interaction of NC with the sensor. Hence, the sensing studies utilizing the I-V response was considered as an effective strategy for quantitative detection of neurological drugs.

View Article Online
DOI: 10.1039/D0NR03427D

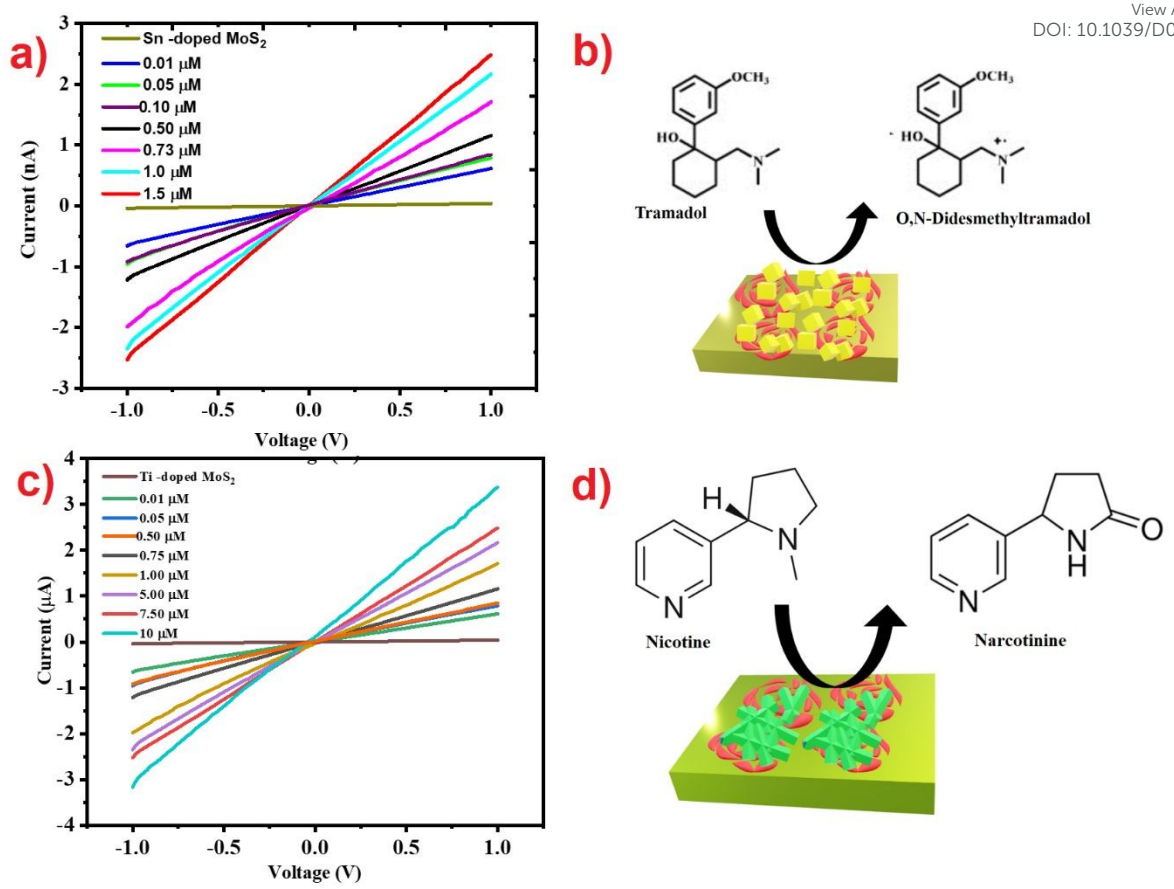

Figure 6 (a) I-V characteristics for various concentration of TR towards Sn-MoS_2 (b) sensing mechanism describing the oxidation of tramadol to O,N- Didesmethyltramadol (c) I-V characteristics for various concentration of NC towards Ti-MoS_2 (d) sensing mechanism describing the oxidation of nicotine to narcotinine.

Real-time detection of neurological drugs in saliva samples:

Amperometric studies were carried out to obtain real time, quick and continuous responses towards various concentration of the 4 neurological drugs by dispersing the drugs in saliva samples (preparation steps given in SI-S2) obtained from a 25-year-old healthy individual. Figure 7(a) displays the real-time amperometric response of the biosensor upon successive spiking of 0.05 µM of AS. The amperometric response followed a decrease in trend of current with increase in concentration of AS. The decrease in current can be attributed to the reduction of acetylsalicylic acid to salicylic acid by withdrawing electrons from the electro-active Al-

View Article Online
DOI: 10.1039/D0NR03427D

MoS_2 as depicted in the sensing mechanism illustrated in figure 5(b). The amperometric studies were carried out at constant reduction potential of AS at 1 V. The calibrated plot for normalised response vs concentration of AS was obtained for (n=5) biosensors as displayed in the inset of figure 7(a). The LOD was calculated as 3S/M, (where S- standard deviation and M – slope of the calibration curve). The linear fitting plots exhibited a sensitivity of 71.96 μM^{-1} and the LOD was measured as 2.90 nM. Figure 7(b) displays the obtained amperometric response of the Cu-MoS_2 biosensor with increase in concentration of CF at a constant oxidation potential of 1 V. An increase in current was observed with increase in concentration of CF. This can be attributed to the oxidation of caffeine by donating electrons to the catalytically active Cu-nanorods decorated MoS_2 nanoflowers as illustrated in figure 5(d). The sensitivity obtained was 41.8 μM^{-1} as displayed in the inset of figure 7(b). The LOD was calculated to be 5.2 nM. The real-time amperometric studies for TR were carried out by dispersing 1 µM of TR in the prepared saliva solution. Figure 7(c) denotes the amperometric response of the Sn-MoS_2 biosensor towards successive spiking of 1 µM of TR. The amperometric response studies were studied at a constant oxidation potential of 1 V. TR undergoes oxidation in presence of TR selective Sn-nanocubes to form O, N – didesmethyltramadol. The sensitivity of the sensor was obtained as 33.27 μM^{-1} as displayed in the inset of figure 7(c) and the LOD was calculated to be 6.31 nM. Finally, the real-time sensing response for NC was obtained by successive spiking 1 µM of NC dispersed in prepared saliva solutions on the Ti-MoS_2 biosensor at a constant oxidation potential of 1 V. Figure 7(d) displays the real-time amperometric response of the sensor to increasing concentrations of NC. The increase in current observed is due to the oxidation of NC to narcotinine by donating electrons to the sensor in presence of catalytic Ti-MoS_2 nano-sticks. The sensitivity obtained was 78.82 μM^{-1} as illustrated in the inset of figure 7(d). The LOD obtained was 2.6 nM. These measurements were repeated for 5 devices (N= 5) and it was seen that the X:MoS_2 biosensors displayed excellent repeatability towards reliable real-time

monitoring of the oral-therapeutic neurological drugs in saliva samples. The obtained statistical data is summarised in the SI. Table S4.

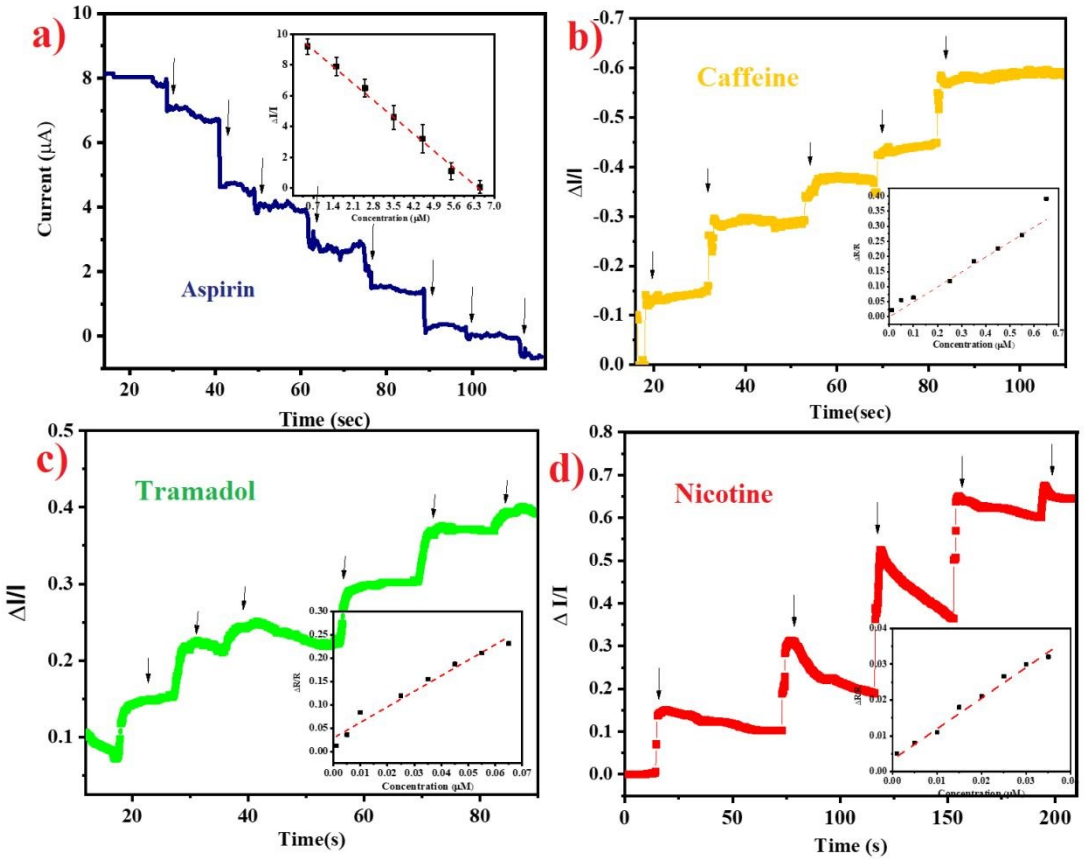

Figure 7(a) Amperometric studies obtained for successive spiking of increase in concentration of : (a) AS inset: calibration plot for increase in concentration of AS b) CF : calibration plot for increase in concentration of CF c) TR inset: calibration plot for increase in concentration of TR d) NC inset: calibration plot for increase in concentration of NC. (N= 5 devices in each case)

Selectivity of the fabricated Biosensor array: -

The selectivity studies of the neurological drug biosensor were carried out to investigate the ability of the biosensor array to yield reliable detection of the 4 drugs in real saliva samples and for studying the effects of screening against possible interfering species. The normalised

response of the biosensor was recorded for each sensor towards the major interfering analytes that exist in saliva like K^+, Na^+, Mg^{2+}, Ca^{2+}, UA and LA along with the neurological drugs for n=5 devices. The physiological range of K^+, Na^+, Mg^{2+}, Ca^{2+}, UA, LA in saliva are found to be 0.16 - 1 mM, 6-8 mM, 0.61-0.9 mM, 0.45- 0.9 mM, 2.95 - 5 mM, 0.2 -0.4 mM respectively [32-35]. Hence, interference experiments were carried out by spiking 10-fold of the reported physiological range to analyse the selectivity of the sensor towards neurological drugs. The resistance of each sensor was obtained in the air (R1) and was also obtained after the drop-casting (R2) of the analytes. The normalized resistance was calculated by using the formula - (R1-R2/R1). Figure 8(a) displays the interference studies of Al-MoS_2 device towards K^+, Na^+, Mg^{2+}, Ca^{2+}, UA, LA and AS. The biosensor displayed excellent response towards AS, which can be attributed to the selectivity of Al-MoS_2 towards AS as evident from PCA analysis. The selectivity of the biosensor can be explained with the help of charge transfer mechanism. AS being highly acidic in nature tends to withdraw electrons from the surface of the Al-MoS_2 device whereas the electropositive metals like K^+, Na^+, Mg^{2+}, Ca^{2+} tend to lose electrons to form positive ions [36] and the normalised resistance is positive in nature evidently proving negligible interference. Figure 8(b) displays the interference studies of Cu-MoS_2 towards K^+, Na^+, Mg^{2+}, Ca^{2+}, UA, LA and CF. The results displayed high selectivity towards CF and negligible response towards analytes. This is due to the alkaloid nature of CF, which is generally observed to be basic in nature consisting of OH^- ions [37]. The OH^- ions donate electrons to the Cu-MoS_2 which further increases the current flowing through the device. However, very weak response was obtained for electropositive metals K^+, Na^+, Mg^{2+}, Ca^{2+}, which can be attributed to the decreased possible charge transfer mechanism due to the least-catalytic behaviour of Cu-nanorods [38] towards the analytes. UA and LA are weak acids consisting of fewer H+ ions, when interacted with the biosensor withdraws least electrons displaying negligible interference with the CF towards Cu-MoS_2. Figure 8(c) displays the

View Article Online
DOI: 10.1039/D0NR03427D

interference studies of Sn-MoS_2 biosensor towards the analytes. The Sn-MoS_2 biosensor was found to be electroactive towards the TR. TR, basically a conjugate base tends to gain or absorb H+ ions when spiked into the biosensor. Hence, the current flowing through the biosensor increases with the spiking of TR, whereas UA and LA donate H+ ions [39] to the biosensor, clearly stating the non-interfering nature of UA and LA in the saliva samples. The interfering species like K^+, Na^+, Mg^{2+}, Ca^{2+} are electropositive metals which lose electrons to the biosensor which further indicates a very small positive normalised resistance value not interfering with the response of the TR sensing. Figure 8(d) displays the interference studies for Ti-MoS_2 towards NC and other interfering analytes. NC, a known alkaloid donates electrons [40] to Ti-MoS_2 which in turn increases the electron flow through the biosensor. However, UA and LA are weak acid which withdraw electrons from the biosensor and thus do not display any interfering effect. Similarly, the electropositive species K^+, Na^+, Mg^{2+}, Ca^{2+} exhibit a very low positive normalised resistance thus not interfering with the response of NC. The biosensor array thus displayed excellent specificity towards the neurological drugs in real saliva samples. When measured aliquot of 0.1 μM - AS, CF, TR, and NC were mixed and spiked on to the fabricated biosensor array, separate signals from each contact were obtained. The PCA analysis was performed and the presence of each analyte was validated as shown in figure S8. The obtained normalised resistance was mapped with the calibrated current values to acquire the concentration of the neurological drugs as displayed in Table S5. Thus, affirming the simultaneous sensing ability of the fabricated biosensor array.

View Article Online
DOI: 10.1039/D0NR03427D

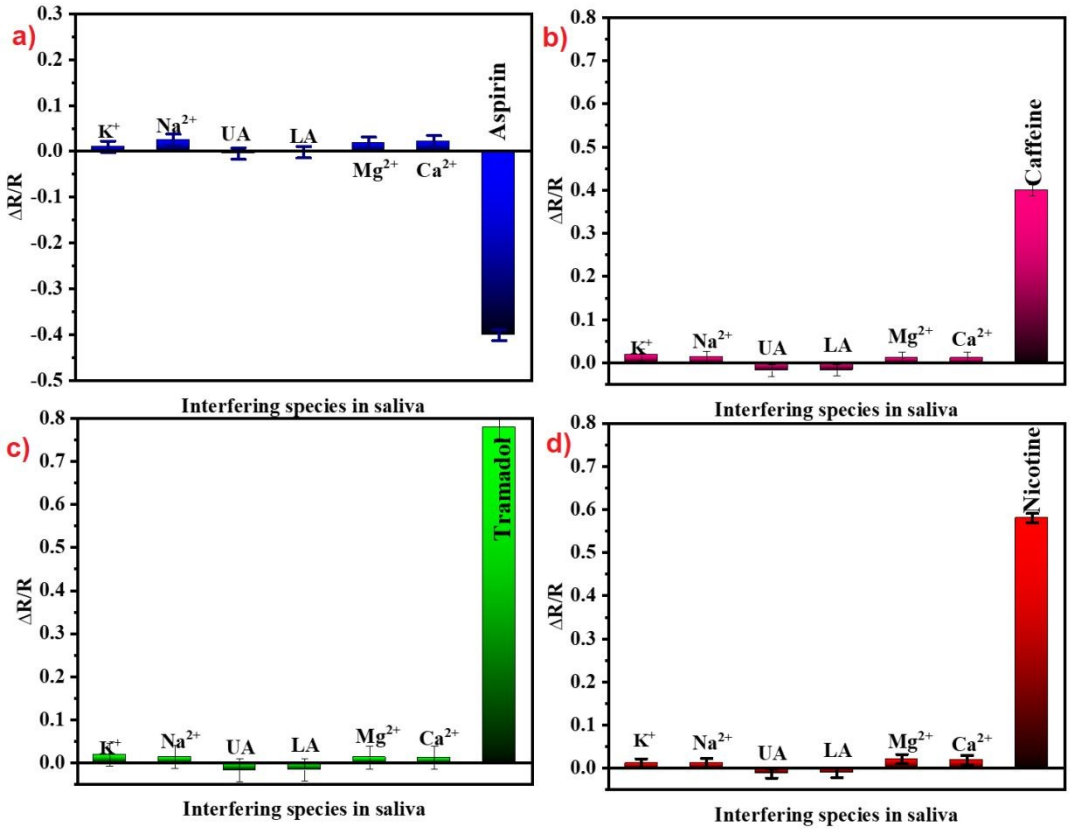

Figure 8(a) The interference studies of the a) Al-MoS_2 b) Cu-MoS_2 c) Sn-MoS_2 and d) Ti-MoS_2 towards interfering species in real time saliva samples (n=5 devices).

Reproducibility and stability of the Biosensor array:

The reproducibility of the sensor was investigated by spiking same concentrations of neurological drugs on the N=5 different sensors. The response of the sensor was recorded as displayed in the table S1 in SI. The relative standard deviation was observed as 0.5 %, 0.67%, 0.637%, 0.502% respectively for AS, CF, TR and NC. The standard deviation was observed to be very less showing excellent repeatable response of the biosensor. The stability studies of the biosensor were performed by recording the response of the device at regular intervals for the duration of four weeks. The response of the biosensor is illustrated in table S2. The relative standard deviation was observed to be < 5.2% for the proposed architecture of the biosensor. The morphology of the X-MoS_2 was found to be almost same even after several times of

sensing as shown in figure S9. This can be attributed to the strong interaction between metal ions and MoS_2 nanostructure. The fabricated biosensor array displayed excellent reproducibility and stability for n-5 different devices.

Table 2. Comparison of the performance of the fabricated Biosensor array with the state of art sensors detection of neurological drugs

Material	Synthesis technique	Method of detection	Neurological drugs	Sensitivity ($\mu A\ \mu M\ cm^{-2}$)	LOD	Integrated E-tongue device	Reference
Surfactant-modified multiwalled carbon-nanotube	Chemical synthesis	Voltammetry	AS CF	-	$8.47x10^{-8}$ M $8.83x10^{-8}$M	No	[40]
Graphene oxide	Mechanical exfoliation	Voltammetry	CF	0.028	3.4 μM	No	[41]
Au/graphene nanosheet	Hummers method, chemical synthesis	Voltammetry	TR	-	0.82 μM	No	[42]
Nitrogen-doped graphene sheets	Hummers method, chemical synthesis	Amperometry	NC	62.7	0.27 μM	No	[43]

X(Metal: Al, Cu, Sn, Ti) functionalized MoS_2	**Hydrothermal**	**Amperometry**	**AS** **CF** **TR** **NC**	**71.96** **41.8** **33.27** **78.82**	**2.90 nM** **5.2 nM** **6.31 nM** **2.6 nM**	**Yes**	**[This work]**

Electrochemical techniques have been used for the quantitative analysis of specific therapeutic neurological drugs. Hence, in this work, a versatile, multifunctional platform for detection of neurological drugs was employed. Table 2 shows the comparison of the as- fabricated E-tongue based biosensor array for detection of neurological drugs with the state of art nanomaterials based sensors. Surfactant-modified multiwalled carbon-nanotube [40] sensor was used for AS and CF sensing, where the binders like nafion was used which reduces the sensitivity of the sensor and moreover the sensor was used on electrochemical platform using rigid electrodes. Further, neurological drugs were electrochemically detected using graphene [41], nitrogen doped graphene [43] and Au/graphene nanosheets [42]. The major limitations with electrochemical methods are complications in electrode synthesis, signal and background current drifts due to fouling and charging effects and the lack of a strategy for simultaneous detection of multiple targets. In this work, metal functionalized MoS_2 nanoflowers have been grown on a biodegradable aluminium substrate and used as a sensing platform. The detection of neurological drugs has been examined qualitatively and quantitatively using multivariate PCA analysis, I-V and amperometric studies. The biosensor array was highly stable and reproducible for more than 28 days. The response for simultaneous detection of multiple targets where carried out using PCA analysis. The versatile biosensor array was found to be highly selective and sensitive towards the neurological drugs like AS, CF, TR and NC with a wide window of dynamic detection range and ultra-low limit of detection. Further, this strategy can

be employed in designing wearable biosensors for detection of various neurological drugs in biofluids for simultaneous detection of multiple targets.

Conclusion:

In summary, X functionalized MoS_2 nanoflowers based neurological drugs detection biosensor array was efficiently developed on a low cost- aluminium substrate. Detailed study revealed that this is the first of its kind report on detection of vital neurological drugs in real-time using human saliva. The biosensor was categorically used for sensing AS, CF, TR and NC using effective statistical analysis and sensing strategies. The biosensor array displayed versatility, high sensitivity, selectivity, stability and reproducibility towards neurological drugs. Thus, this report paves a path towards reproducible, flexible and wearable biosensors for detection of vital neurological drugs in bio-fluids.

Conflict of interest

There are no conflicts to declare

Acknowledgment

SB acknowledges financial assistance from Scientific and Engineering Research Board (SERB) grant SB/WEA-03/2017

References:

[1] Adil, M. M., Rao, A. T., Ramadoss, G. N., Chernavsky, N. E., Kulkarni, R. U., Miller, E. W., ... & Schaffer, D. V. *Adv. Func. Mater.*, 2018, *28*(41), 1804144. https://doi.org/10.1002/adfm.201804144

[2] Rabie, H., Zhang, Y., Pasquale, N., Lagos, M. J., Batson, P. E., & Lee, K. B. *Adv. Mater.*, 2019 *31*(14), 1806991. https://doi.org/10.1002/adma.201806991

[3] Sanghavi, B. J., Wolfbeis, O. S., Hirsch, T., & Swami, N. S. *Microchimica Acta*, 2015 *182*(1-2), 1-41. https://doi.org/10.1007/s00604-014-1308-4

[4] Hulvey, M. K., Lunte, S. M., Fischer, D. J., & Kuhnline, C. D. *Encyclopedia of Analytical Chemistry: Applications, Theory and Instrumentation*. 2006. https://doi.org/10.1002/9780470027318.a9071

[5] Ibañez, F. J., & Zamborini, F. P. *Small*, 2012 *8*(2), 174-202. https://doi.org/10.1002/smll.201002232

[6] Mali, K. S., Greenwood, J., Adisoejoso, J., Phillipson, R., & De Feyter, S. *Nanoscale*, 2015 *7*(5), 1566-1585. https://doi.org/10.1039/C4NR06470D

[7] Lei, S., Wang, X., Li, B., Kang, J., He, Y., George, A., ... & Brunetto, G. *Nat. nanotechnol.*, 2016 *11*(5), 465. . https://doi.org/10.1038/nnano.2015.323

[8] Pentzer, E. B., Bokel, F. A., Hayward, R. C., & Emrick, T. *Adv. Mater.*, 2012 *24*(17), 2254-2258. https://doi.org/10.1002/adma.201104788

[9] Campuzano, S., Pedrero, M., Nikoleli, G. P., Pingarrón, J. M., & Nikolelis, D. P. *Biosens. Bioelectron.*, 2017 *89*, 269-279. https://doi.org/10.1016/j.bios.2016.01.042

[10] Thompson, G. E., Furneaux, R. C., Wood, G. C., Richardson, J. A., & Goode, J. S. *Nature*, 1978 *272*(5652), 433. https://doi.org/10.1038/272433a0

[11] Yu, X., Yu, J., Cheng, B., & Jaroniec, M. *J. Phys. Chem. C*, 2009 *113*(40), 17527-17535. https://doi.org/10.1021/jp906992r

[12] Lahtonen, K., Hirsimäki, M., Lampimäki, M., & Valden, M.. *J. chem. phys.*, 2008 *129*(12), 124703. https://doi.org/10.1063/1.2980347

View Article Online
DOI: 10.1039/D0NR03427D

[13] Xi, G., & Ye, J. *Inorg. Chem.*, 2010 *49*(5), 2302-2309. https://doi.org/10.1021/ic902131a

[14] Baldim, V., Bia, N., Graillot, A., Loubat, C., & Berret, J. F.. *Adv. Mater. Interf.s*, *6*(7), 1801814. https://doi.org/10.1002/admi.201801814

[15] Teich, J., Dvir, R., Henning, A., Hamo, E., Moody, M. J., Cohen, H. & Ismach, A. (2020). *Nanoscale*. https://doi.org/10.1039/C9NR09564K

[16] Rastogi, P. K., Sarkar, S., & Mandler, D.*Appl. Mater. Today*, 2017 *8*, 44-53. https://doi.org/10.1016/j.apmt.2017.04.004

[17] Zhu, D., Liu, J., Zhao, Y., Zheng, Y., & Qiao, S. Z. *Small*, 2019 *15*(14), 1805511. https://doi.org/10.1002/smll.201805511

[18] Yin, L. W., Bando, Y., Zhu, Y. C., Golberg, D., & Li, M. S. *Advanced Materials*, 2004 *16*(11), 929-933. https://doi.org/10.1002/adma.200306571

[19] Zhu, L., Zhao, Y., Zheng, W., Ba, N., Zhang, G., Zhang, J., ... & Bie, L. *CrystEngComm*, 2016 *18*(27), 5202-5208. https://doi.org/10.1039/C6CE00370B

[20] Shakya, J., Kumar, S., Kanjilal, D. *Sci Rep* **7,** 9576 (2017). https://doi.org/10.1038/s41598-017-09916-5

[21] Navas, J., Sánchez-Coronilla, A., Gallardo, J. J., Hernández, N. C., Piñero, J. C., Alcántara, R., ... & Martín-Calleja, J. *Nanoscale*, 2015 *7*(14), 6216-6229. https://doi.org/10.1039/C5NR00041F

[22] He, K., Wen, Q., Wang, C., Wang, B., Yu, S., Hao, C., & Chen, K.. *Chemical Engineering Journal*, 2018 *349*, 416-427. https://doi.org/10.1016/j.cej.2018.05.102

[23] Yan, Y., Ge, X., Liu, Z., Wang, J. Y., Lee, J. M., & Wang, X. *Nanoscale*, 2013 *5*(17), 7768-7771. https://doi.org/10.1039/C3NR02994H

[24] Lordkipanidzé, M., Pharand, C., Schampaert, E., Turgeon, J., Palisaitis, D. A. & Diodati, J. G. *Eur. heart J*, 2007 *28*(14), 1702-1708. https://doi.org/10.1093/eurheartj/ehm226

[25] Guo, S., Wen, D., Zhai, Y., Dong, S., & Wang, E. *ACS nano*, 2010 *4*(7), 3959-3968. https://doi.org/10.1021/nn100852h

[26] Tassaneeyakul, W., Birkett, D. J., McManus, M. E., Tassaneeyakul, W., Veronese, M. E., Andersson, T., ... & Miners, J. O. (1994). *Biochem. Pharmacol.*, *47*(10), 1767-1776. https://doi.org/10.1016/0006-2952(94)90304-2

[27] van Dyk, M., Miners, J. O., Marshall, J. C., Wood, L. S., Hopkins, A., Sorich, M. J., & Rowland, A. *Eur. j. clin. pharmacol.*, 2019 1-8. https://doi.org/10.1007/s00228-019-02682-5

[28] Stoops, W. W., Glaser, P. E., & Rush, C. R. *Psychopharmacol.*, 2013 *228*(2), 255-262. https://doi.org/10.1007/s00213-013-3031-y

[29] Vlase, L., Leucuta, S. E., & Imre, S. *Talanta*, 2008 *75*(4), 1104-1109. https://doi.org/10.1016/j.talanta.2008.01.006

[30] Jacob, N., Golmard, J. L., & Berlin, I. *Acta Paediatrica*, 2015 *104*(8), e360-e366. https://doi.org/10.1111/apa.13031

[31] Highton, L., Kadara, R. O., Jenkinson, N., Logan Riehl, B., & Banks, C. E. *Electroanalysis*, 2009 *21*(21), 2387-2389. https://doi.org/10.1002/elan.200904683

[32] Urbanowicz, M., Jasiński, A., Jasińska, M., Drucis, K., Ekman, M., Szarmach, A., & Bocheńska, M. 2017. *Electroanalysis*, *29*(10), 2232-2238.

[33] Shibasaki, K., Kimura, M., Ikarashi, R. *Metabolomics* **8,** 484–491. 2012.

[34] Palleschi, G., Faridnia, M. H., Lubrano, G. J., & Guilbault, G. G. (1991). *Analytica chimica acta*, *245*, 151-157.

[35] Aziz, N. Z., Arathi, K., Prasad, B. G., Desai, D., Shetty, S. J., & Shahid, M. *Journal of oral and maxillofacial pathology: JOMFP*, *22*(1), 147.

[36] Ceja-Navarro, J. A., Vega, F. E., Karaoz, U., Hao, Z., Jenkins, S., Lim, H. C., ... & Brodie, E. L. *Nat. commun.*, 2015 *6*, 7618. https://doi.org/10.1038/ncomms8618

[37] Wang, X., Chen, S., Reggiano, G., Thota, S., Wang, Y., Kerns, P., ... & Zhao, J. *Chem. Commun.*, 2019 *55*(9), 1249-1252. https://doi.org/10.1039/C8CC08083F

[38] Veeralingam, S., & Badhulika, S. *Mat Sci Eng C-Mater.,* 2019 110365. https://doi.org/10.1016/j.msec.2019.110365

[39] Zhao, Z., Hu, Y., Harmon, T., Pentel, P. R., Ehrich, M., & Zhang, C. Nanomed. Nanotechnol., 2018 *14*(5), 1655-1665. https://doi.org/10.1016/j.nano.2018.04.016

[40] Sanghavi, B. J., & Srivastava, A. K. *Electrochim. Acta*, 2010 *55*(28), 8638-8648. https://doi.org/10.1016/j.electacta.2010.07.093

[41] Raj, M. A., & John, S. A. *Analytica chim. acta*, 2013 *771*, 14-20. https://doi.org/10.1016/j.aca.2013.02.017

[42] Xu, J., Wang, Y., & Hu, S. (2017). *Microchimica Acta*, *184*(1), 1-44.

[43] Li, X., Zhao, H., Shi, L., Zhu, X., Lan, M., Zhang, Q., & Fan, Z. H.. *J. Electroanalyt. Chem.*, 2017 *784*, 77-84. https://doi.org/10.1016/j.jelechem.2016.12.009

View Article Online
DOI: 10.1039/D0NR03427D

Graphical Abstract: